nature biomedical engineering

Article

https://doi.org/10.1038/s41551-022-00977-0

Systemic enhancement of antitumour immunity by peritumourally implanted immunomodulatory macroporous scaffolds

In the format provided by the authors and unedited

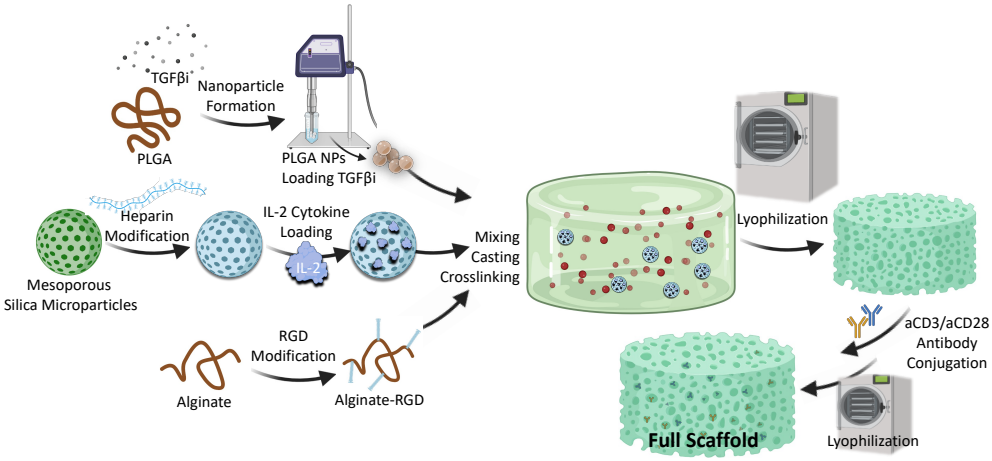

Supplementary Fig. 1 l Schematic representation of scaffold components and fabrication steps.

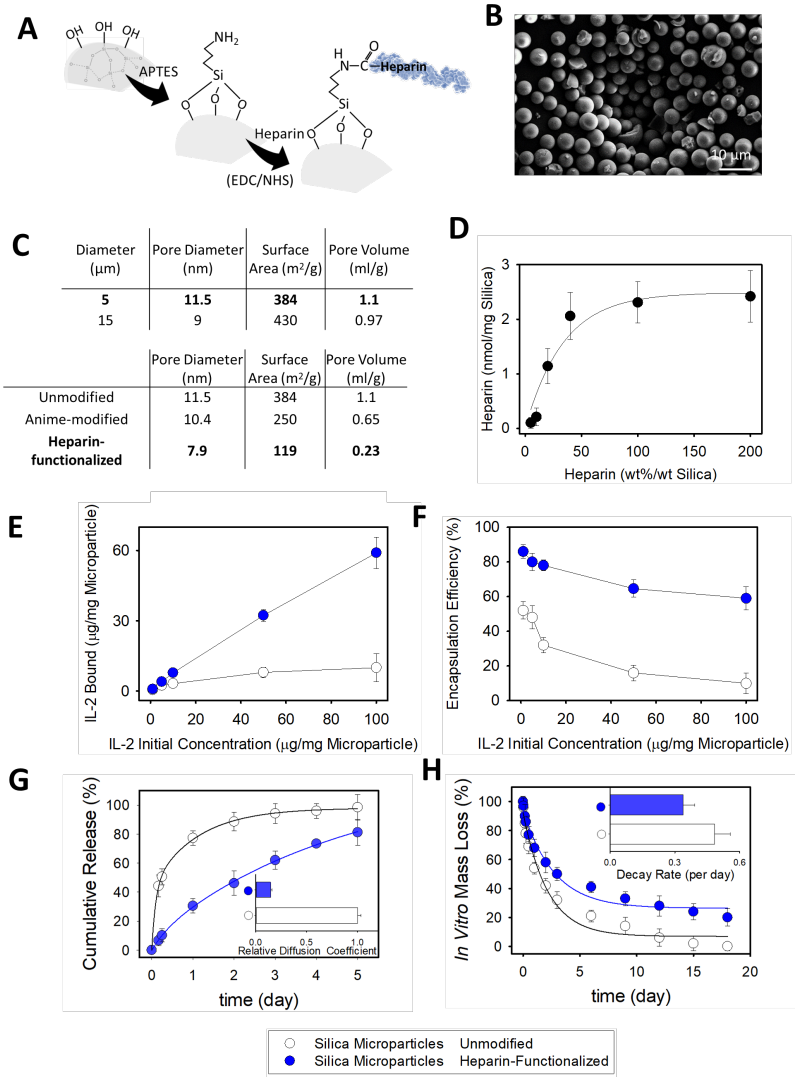

Diameter (μm)	Pore Diameter (nm)	Surface Area (m^2/g)	Pore Volume (ml/g)
5	**11.5**	**384**	**1.1**
15	9	430	0.97

	Pore Diameter (nm)	Surface Area (m^2/g)	Pore Volume (ml/g)
Unmodified	11.5	384	1.1
Anime-modified	10.4	250	0.65
Heparin-functionalized	**7.9**	**119**	**0.23**

Supplementary Fig. 2 l IL-2 cytokine is released from heparin-coated mesoporous silica microparticles. **(a)** Surface chemistry for conjugation of heparin. **(b)** SEM image of synthesized mesoporous microparticles. **(c)** Change in physical characteristics of mesoporous silica microparticles after surface functionalization with APTES and heparin. **(d)** The degree of heparin-conjugation of silica particles with various initial amounts of heparin in the reaction mixture. **(e)** Binding efficiency of IL-2 to the unmodified compared to heparin-functionalized microparticles. **(f)** Encapsulation efficiency of IL-2 in unmodified compared to heparin-functionalized microparticles as a function of initial IL-2 concentration. **(g)** Cumulative release of IL-2 from heparin-functionalized and unmodified silica microparticles at 37 °C. (inset) calculated diffusion coefficients. **(h)** In vitro degradation of silica-based microparticles over time. (**e-h**) unmodified (open circles) compared to heparin modified (blue-filled circles) microparticles.

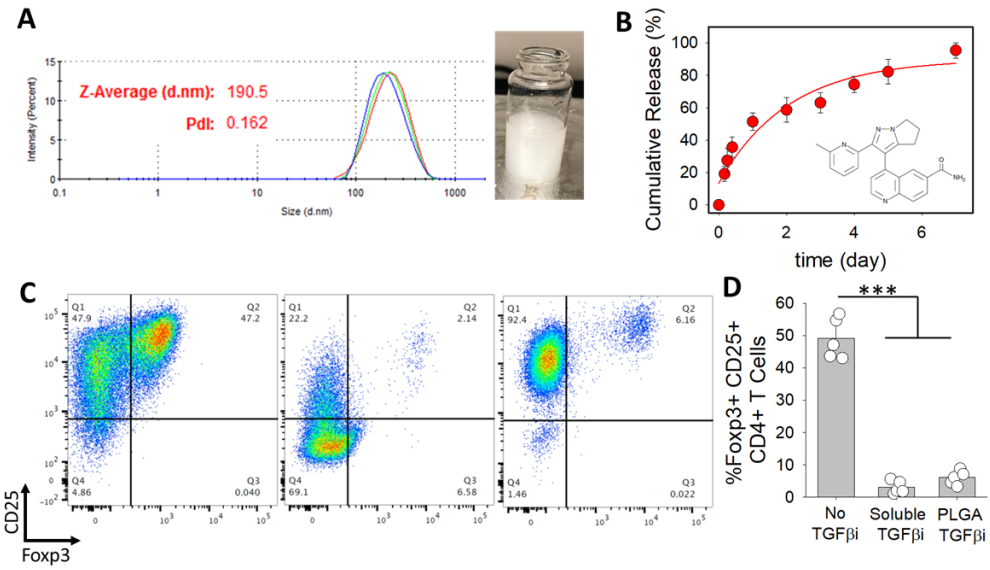

Supplementary Fig. 3 l PLGA nanoparticles loaded with TGF-βi. (A) Dynamic light scattering (DLS) showing monodisperse formation of TGF-βi-loaded PLGA nanoparticles. Inset showing stable suspension of formed nanoparticles in water 24 h after dispersion. **(B)** Release of TGF-βi from nanoparticles over time at 37 °C. Chemical structure of selected TGFbi, LY2157299, was also shown. **(C)** Left- Activation of naïve helper T cells results in formation of Tregs, using anti-CD3/28-coated aAPCs in the presence of soluble TGF-β. Middle- Inhibition of Treg formation using soluble TGF-βi (10 μM) or PLGA NPs loaded with equivalent amounts of TGF-βi. **(D)** Quantified percentages of formed Tregs.

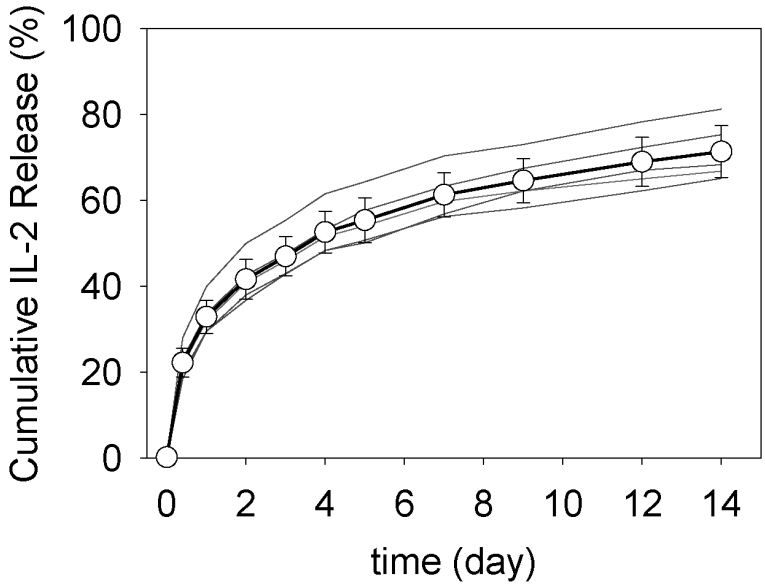

Supplementary Fig. 4 | IL-2 release from scaffolds. Release of IL-2 encapsulated within mesoporous silica microparticles embedded in the alginate 3D scaffold. The released IL-2 was measured by ELISA over time under gentle shaking (50 rpm) at 37 °C.

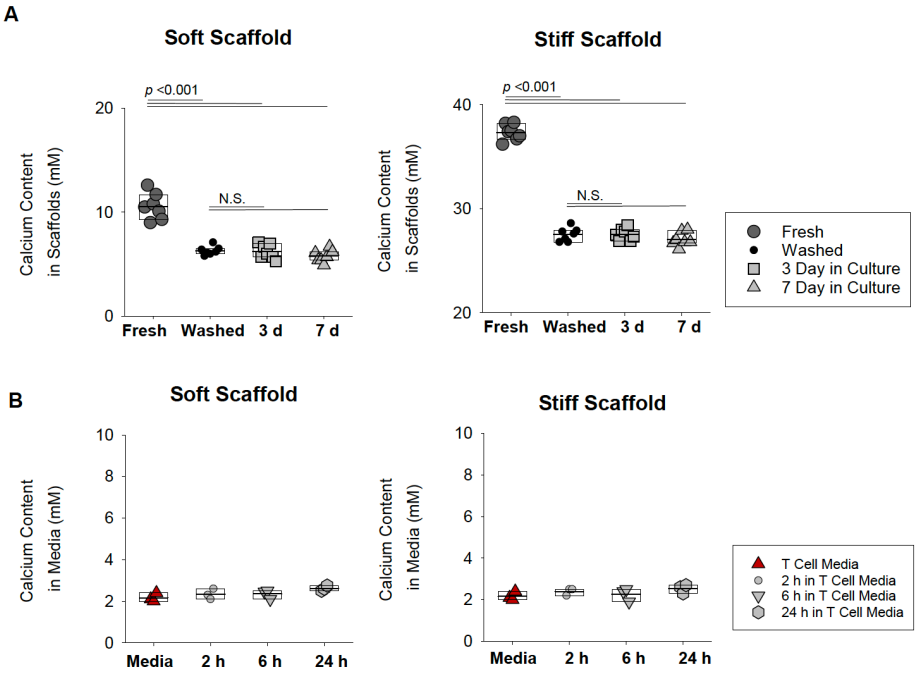

Supplementary Fig. 5 l A. Change in the calcium content of alginate-based scaffolds themselves following extended washing in PBS, and the subsequent incubation in T-cell media. At various times shown, the calcium content released from lysis of the scaffold were measured. Each data point represents an independent scaffold (n=5). **B.** We also measured the amount of calcium leaching into the media from three scaffolds of two stiffnesses after immersion in T-cell media for 2, 6 and 24 hours (new section B of the figure below). We compared these calcium concentrations to media alone. There were no differences in calcium concentration across any of the conditions.

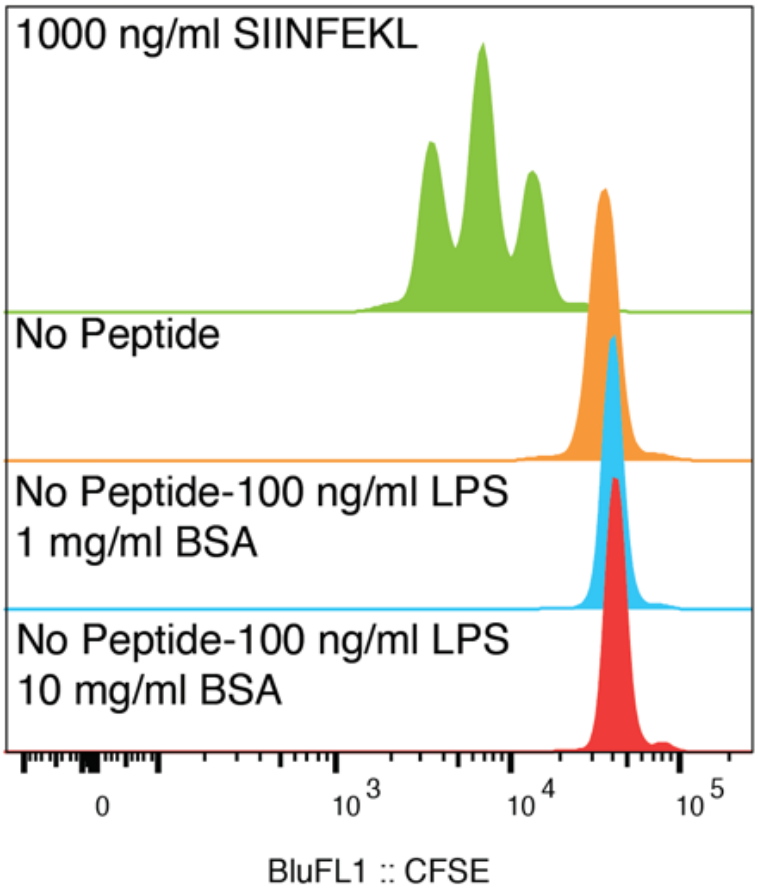

Supplementary Fig. 6 l Presence of BSA in the formulation does not affect T cell activation. Naïve OT1 CD8+ primary mouse T cells co-cultured with Ovalbumin antigen (SIINFEKL) as a positive control or BSA (1 and 10 mg/ml) in the presence of LPS (100 ng/ml). Flow cytometry analysis of cell division (CFSE dilution) assayed three days after treatment of T cells with the above mentioned formulations.

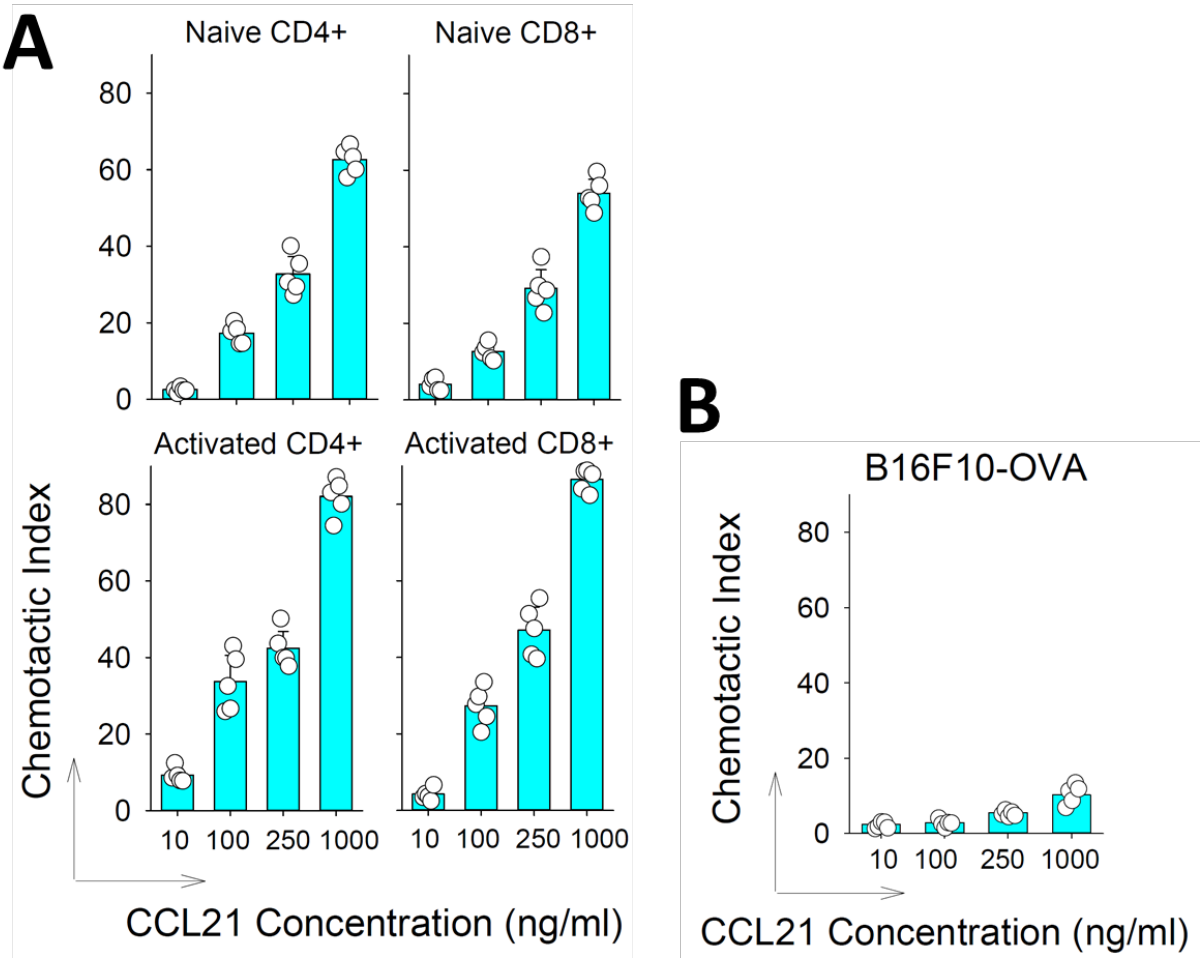

Supplementary Fig. 7 l Assessment of CCL21 chemotaxis in recruitment of **(A)** naive and activated CD4+ and CD8+ T cells and **(B)** B16F10-OVA tumor cells *in vitro*. 5×10^5 naive or activated T cells were loaded on the top filter of the transwell chamber. Hydrogels containing various concentrations of recombinant CCL21 were placed in the bottom wells at the indicated concentrations. Viable cells migrating to the lower chamber after 4 h (T cells) or 8 h (B16 cells) were quantified after digesting the scaffold. Chemotactic Index: fold migration over background (empty scaffolds). 5 μm pore size was selected for Transwell migration assay.

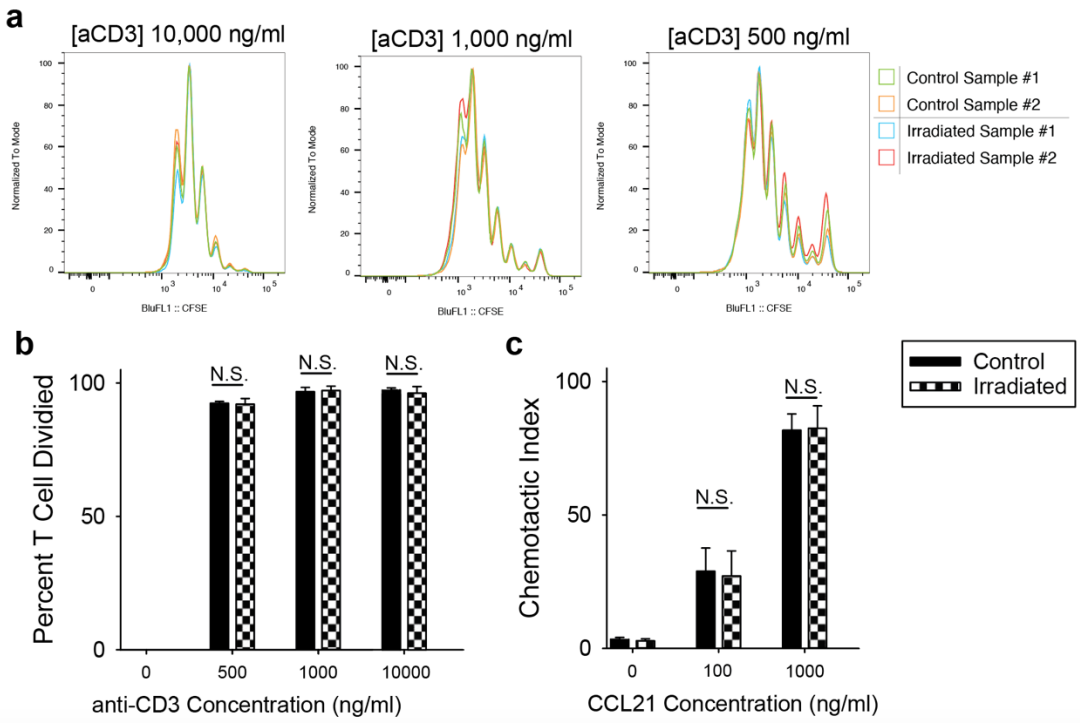

Supplementary Fig. 8 l X-ray irradiation (sterilization) will not affect the functionality of IL-2 cytokine, CCL21 chemokine, and aCD3/aCD28 antibodies. (a) Naïve CD8+ mouse T cells cultured with control and irradiated IL-2 cytokine and aCD3/aCD28 antibodies. Flow cytometry analysis of cell division (CFSE dilution) assayed three days after treatment of the T cells with the above mentioned formulations. (b) %Proliferated is the percentage of T cells that divided at least once. (c) **Assessment of CCL21 chemotaxis following irradiation.** 5×10^5 activated CD8+ T cells were loaded on top of the transwell chamber. Hydrogels containing fresh or irradiated recombinant CCL21 were placed in the bottom wells at the indicated concentrations. Viable cells that migrated to the lower chamber after 4 h were quantified after digesting the scaffold. Chemotactic Index: fold migration over background (empty scaffolds). 5 µm pore size was selected for Transwell migration assay.

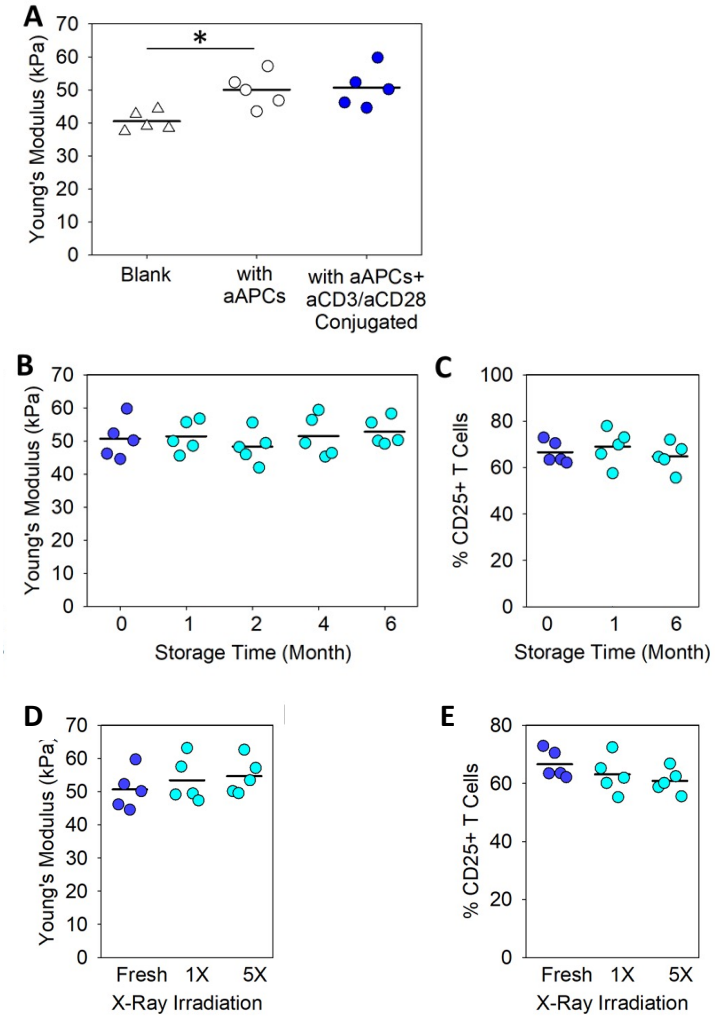

Supplementary Fig. 9 | Mechanical characteristics of the 3D scaffolds. (A) Change in mechanical properties of 3D alginate scaffolds in absence or presence of IL-2 releasing silica-based aAPCs with or without surface coating of the scaffold with anti-CD3/ anti-CD28 antibodies. **(B-C) Shelf-life evaluation of scaffolds.** Freeze-dried hydrogel batches were stored at 4 °C for different durations up to six months and changes in (**B**) mechanical properties were assessed as in A. (**C**) Assessment of activation capability of the 3D scaffold after storage. Scaffolds were prepared with microparticles comprising IL-2-releasing silica microparticles with and without surface coating of the scaffold with anti-CD3/ anti-CD28 antibodies and stored for various durations. Scaffolds were then used for co-culture with naïve, primary CD8+ T cells. Activated T Cells were assessed by upregulated expression of CD25. **(D)** Change in mechanical properties and **(E)** T cell activation of scaffolds after 1 or 5 cycles of x-ray irradiation at 25 kGy dose compared to freshly prepared samples. Lyophilized scaffolds were exposed to X-ray exposures with 24 h time intervals. **(A-E)** Each dot represents an independent experiment (n=5). The results were statistically analyzed using one-way ANOVA with post-hoc analysis. In (B-E) Results showed no statistically significant ($p > 0.05$) changes in elastic modulus or T-cell activation.

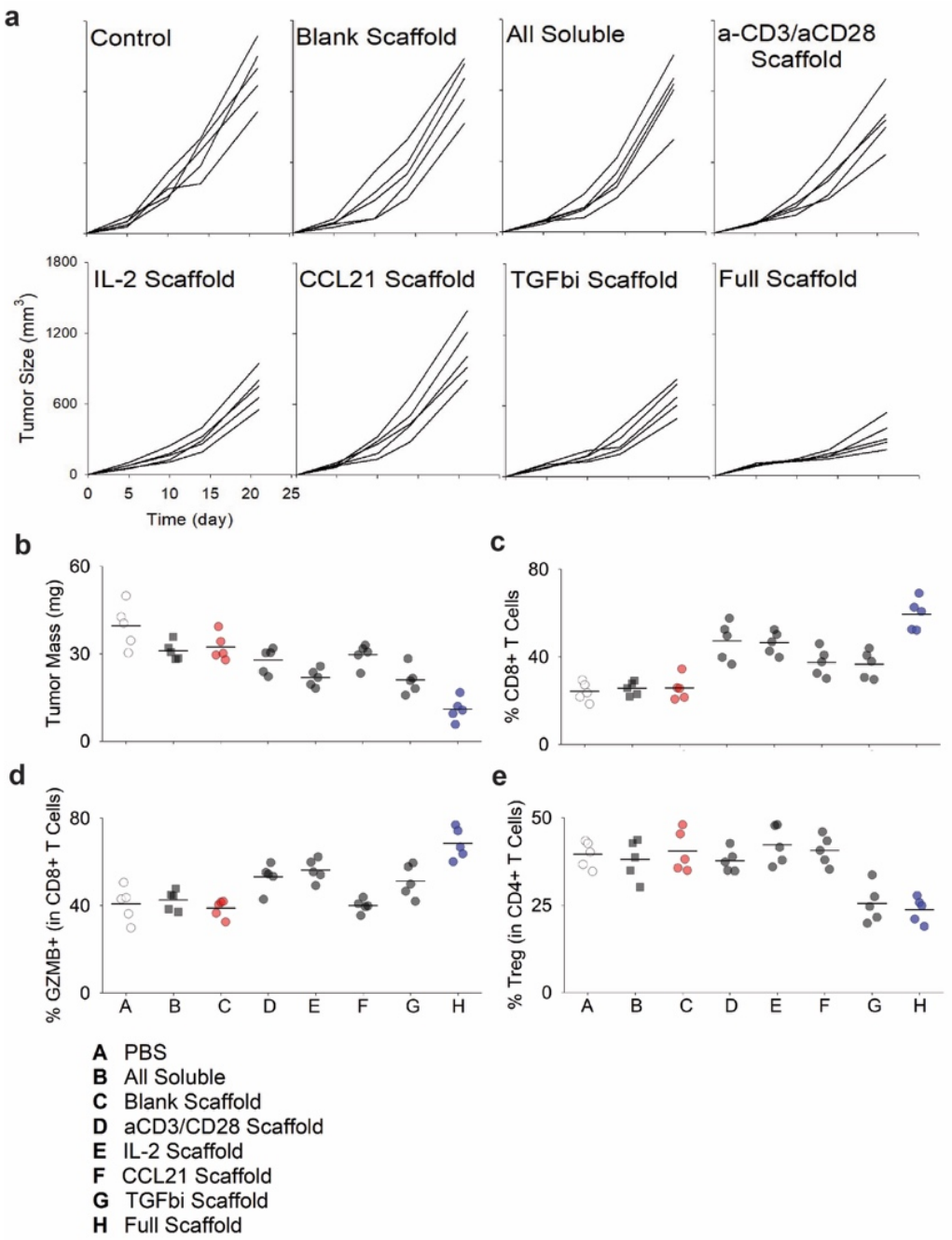

Supplementary Fig. 10 l Individual components cannot accomplish the same tumor suppression as Full scaffolds. 4T1 breast cancer (a) tumor growth and (b) final tumor mass in wild-type mice implanted with either full or control scaffolds that were composed of only one individual component including aCD3/CD28 conjugation, IL-2 loading, CCL21 loading, or TGFbi loading as well as blank scaffolds. The treatment group that received intratumoral injection of all the components in the soluble format is also included here(c) Presence and (d) activation of CD8+ T cells were studied. (e) Frequency of Tregs is also demonstrated in tumor tissues. (n = 5). Each point represents one mouse. Please refer **Supplementary Table 1** for the statistical comparisons.

Supplementary Table 1 l (Related to **Supplementary Fig. 10**) One Way Analysis of Variance (ANOVA) was used for all pairwise multiple comparison using Holm-Sidak method. All data were assessed with Normality Test (Shapiro-Wilk) and Equal Variance Test (Brown-Forsythe). Overall significance level is set to be 0.05.

Comparison	Tumor Mass	Tumor CD8+	Tumor CD8+GZMB+	Tumor Treg (Foxp3+CD25+CD+)
PBS vs. All Sol	NS	NS	NS	NS
PBS vs. Blank	NS	NS	NS	NS
PBS vs. CD3/CD28	0.005	<0.001	0.032	NS
PBS vs. IL-2	<0.001	<0.001	0.005	NS
PBS vs. CCL21	0.024	0.024	NS	NS
PBS vs. TGFbi	<0.001	0.039	NS	0.001
PBS vs. Full	<0.001	<0.001	<0.001	<0.001
All Sol vs. Blank	NS	NS	NS	NS
All Sol vs. CD3/CD28	NS	<0.001	NS	NS
All Sol vs. IL-2	0.042	<0.001	0.016	NS
All Sol vs. CCL21	NS	0.049	NS	NS
All Sol vs. TGFbi	0.023	NS	NS	0.004
All Sol vs. Full	<0.001	<0.001	<0.001	<0.001
Blank vs. CD3/CD28	0.017	<0.001	0.009	NS
Blank vs. IL-2	<0.001	<0.001	0.001	NS
Blank vs. CCL21	NS	NS	NS	NS
Blank vs. TGFbi	<0.001	0.049	0.031	<0.001
Blank vs. Full	<0.001	<0.001	<0.001	<0.001
CD3/CD28 vs. IL-2	NS	NS	NS	NS
CD3/CD28 vs. CCL21	NS	NS	0.021	NS
CD3/CD28 vs. TGFbi	NS	NS	NS	0.005
CD3/CD28 vs. Full	<0.001	0.045	0.005	0.001
IL-2 vs. CCL21	NS	NS	0.003	NS
IL-2 vs. TGFbi	NS	NS	NS	<0.001
IL-2 vs. Full	0.013	0.029	0.036	<0.001
CCL21 vs. TGFbi	NS	NS	NS	<0.001
CCL21 vs. Full	<0.001	<0.001	<0.001	<0.001
TGFbi vs. Full	0.024	<0.001	0.001	NS

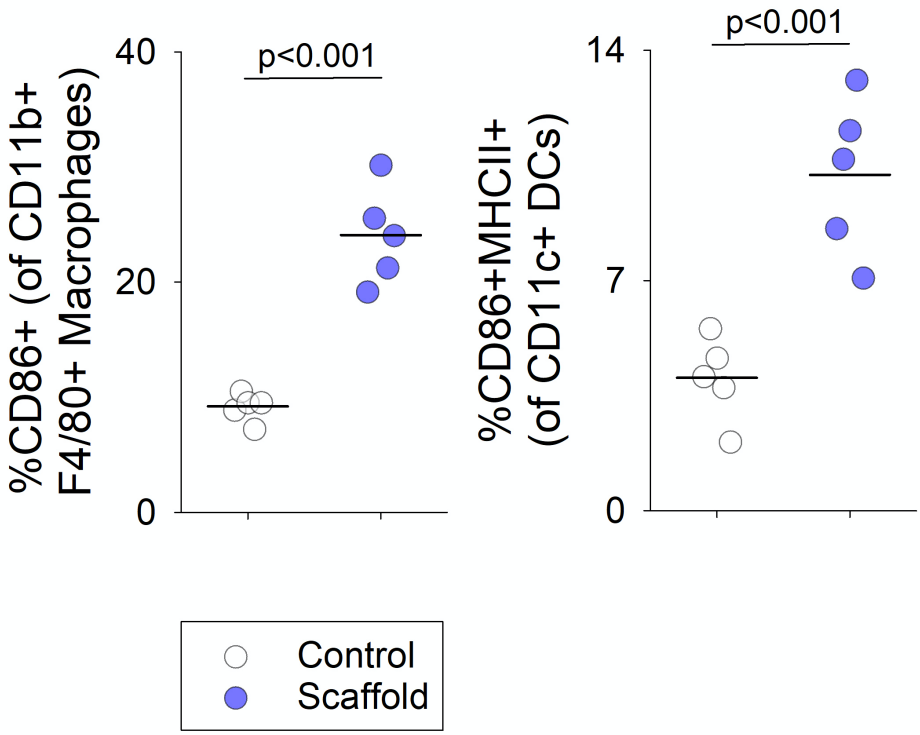

Supplementary Fig. 11 l Population of tumor associated macrophages and dendric cells (DCs). Graphs showing the frequency of activated (CD86+) CD11b+ F4/80+ macrophages and activated (CD86+MHCII+) CD11c+ DCs.

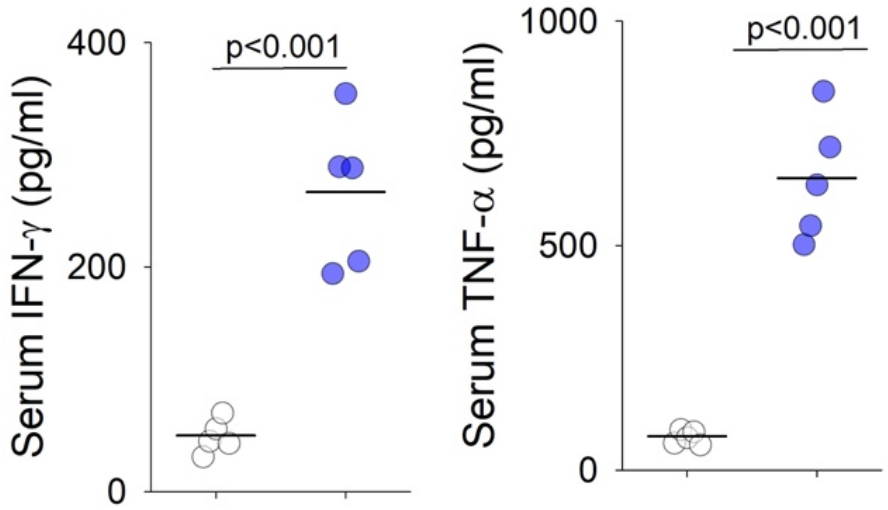

Supplementary Fig. 12 l Serum cytokine concentration. Concentration of IFN-g and TNF-a inflammatory cytokines in mice peripheral blood 7 days post insertion of “Full” scaffolds (blue circles) compared to control mice injected with PBS (open circles).

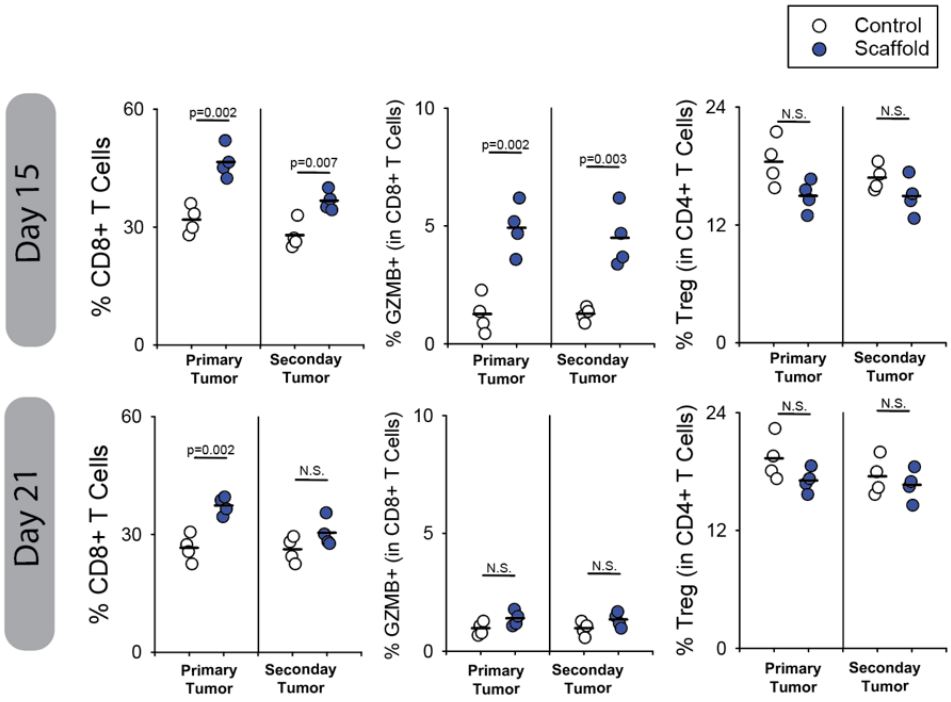

Extended Figure 13 l Secondary breast cancer tumor model, T cell activation <u>in the draining lymph nodes</u>, 15 and 21 days after inoculation of tumor cells using flow cytometry. Percentage of CD8+ T cells found in tumor draining lymph nodes being treated with immunoactive scaffold or PBS control. Frequency of CD8+ T cells with high expression of GZMB and Foxp3+CD25+CD4+ Tregs were measured. (n= 4).

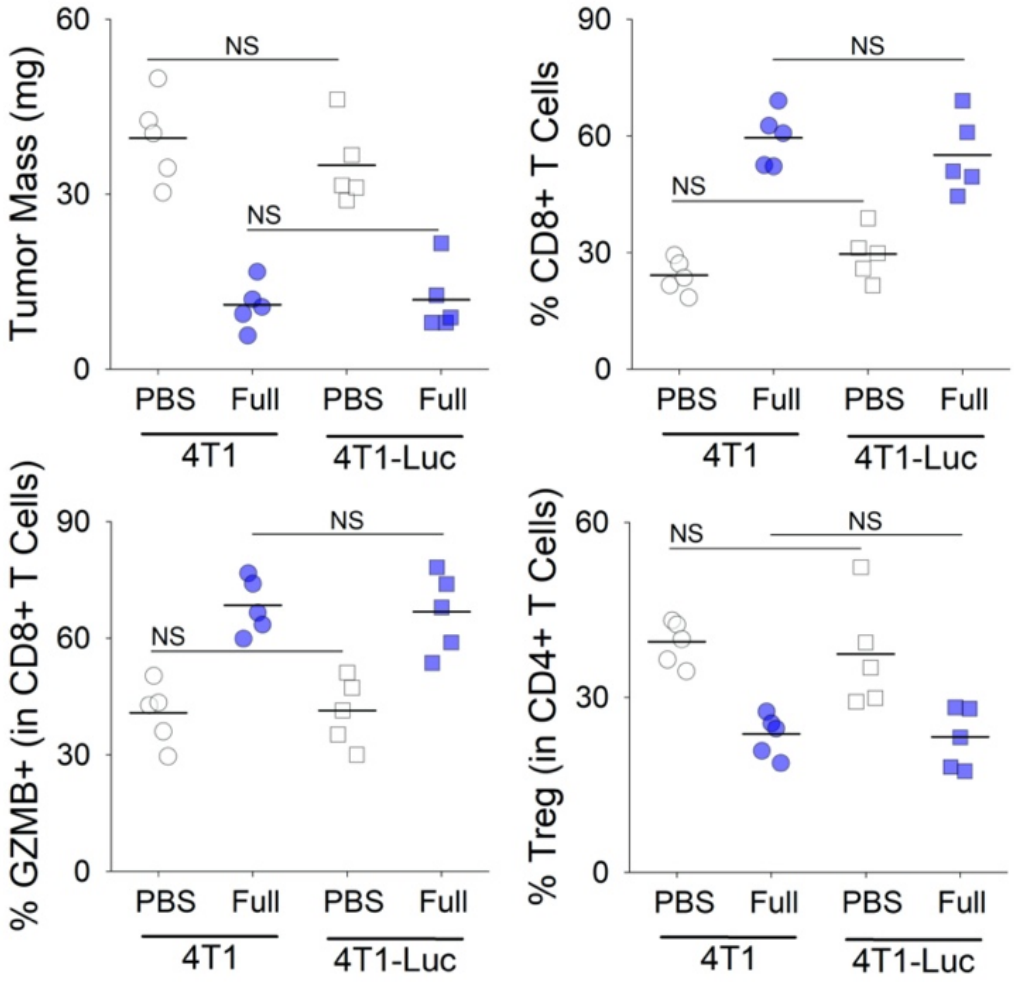

Supplementary Fig. 14 | Presence or absence of Luciferase (Luc) enzyme will not affect progression and response of 4T1 breast cancer cells *in vivo*. Tumor mass on day 15 after mammary fat pad injection of $5x10^5$ 4T1 or 4T1-Luc cancer cells. Frequency of CD8+ T cells and activated CD8+ T cells within tumor microenvironment. Suppression of Tregs in mice bearing 4T1 or 4T1-Luc cancer cells treated with either PBS control or immunoactive scaffolds were also evaluated. Each point represents one mouse.

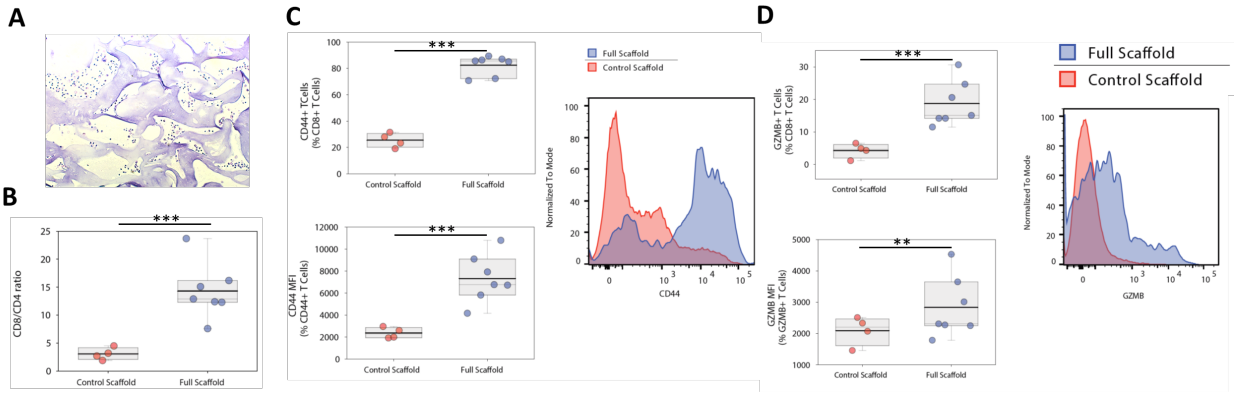

Supplementary Fig. 15 l Activation of endogenous T cells recruited <u>into scaffolds</u>. (A) H&E staining of the cross sections of the subcutaneously implanted scaffolds that originated from the alginate biopolymer, 7 days after implantation. **(B)** FACS quantification of CD8-to-CD4 ratio of recruited T cells extracted from immunoactive ("Full") and control scaffolds. **(C,D)** Flow cytometry analysis of endogenous T cell activation is studied 17 days after subcutaneous implantation of scaffolds. Activation of recruited CD8+ T cells was monitored by measuring surface expression of CD44 as well as intracellular measurement of Granzyme B (GZMB) expression. **(C)** Percentage of T cells with high expression of CD44 and mean fluorescence intensity (MFI) of T cells upregulating CD44 were plotted alongside with representative flow cytometry graphs. **(D)** Percentage of T cells with high intracellular expression of GZMB and MFI of GZMB secreting T cells were plotted. Representative flow cytometry graphs also presented. Each point represents one mouse. Immunoactive scaffold (n = 7) compared with control scaffolds (n = 4).

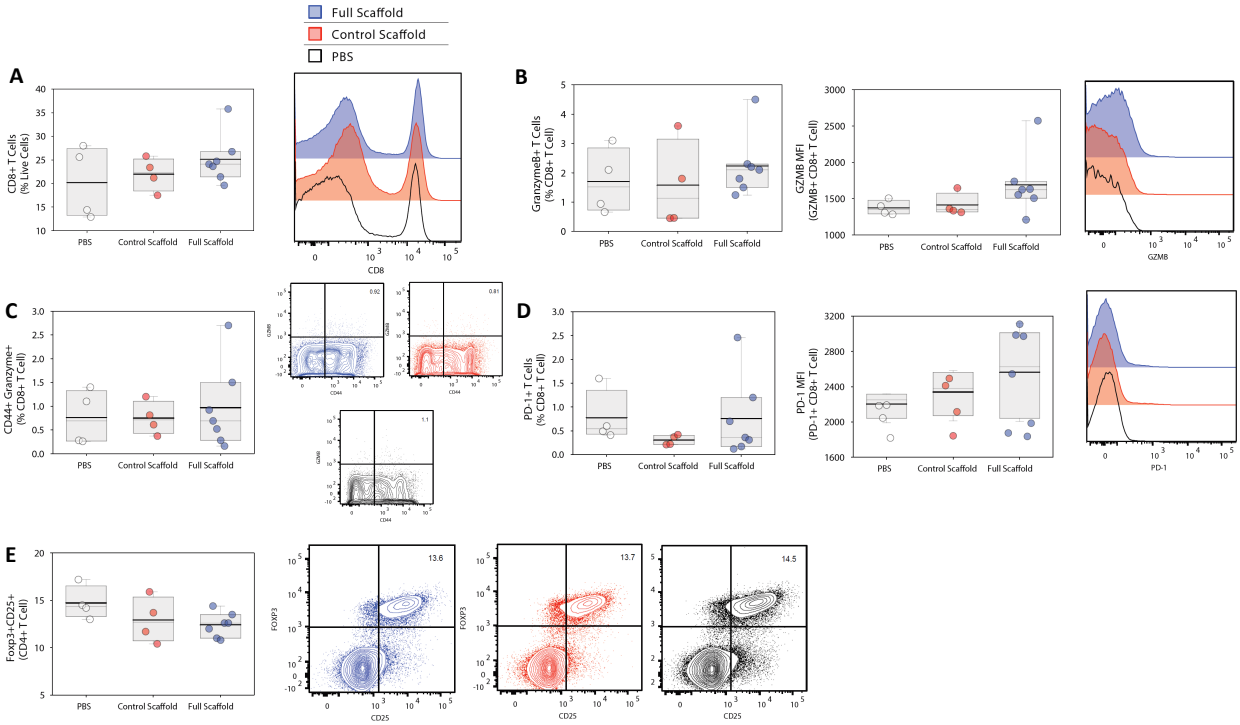

Supplementary Fig. 16 l No major effects on T cells in <u>tumor-draining lymph nodes</u>. (A) Flow cytometry analysis of percentage of CD8+ T cells in tumor draining lymph nodes 22 days after subcutaneous injection of B16F10-ova cells in mice receiving different treatment. **(B-D)** Activation of CD8+ T cells in the tumor draining lymph nodes was monitored by measuring their surface CD44 expression as well as Granzyme B (GZMB) intracellular expression. **(B)** Percentage of T cells with high intracellular expression of GZMB and mean fluorescence intensity (MFI) of T cells upregulating GZMB were plotted alongside with representative flow cytometry graphs. **(C)** Percentage of T cells with high expression of CD44 activation marker and ZMB effector cytokine were plotted. Representative flow cytometry graphs also presented. **(D)** Percentage of PD-1 expressing T cells and their MFIs gated on PD-1+ T cells were plotted. Representative flow cytometry graphs also presented. **(E)** The frequency of Foxp3+CD25+CD4+ Tregs in tumor draining lymph nodes. Representative flow cytometry graphs are shown for mice treated with Immunoactive Scaffolds (Blue), Control Scaffolds (Red), and PBS (Black). Each point represents one mouse.

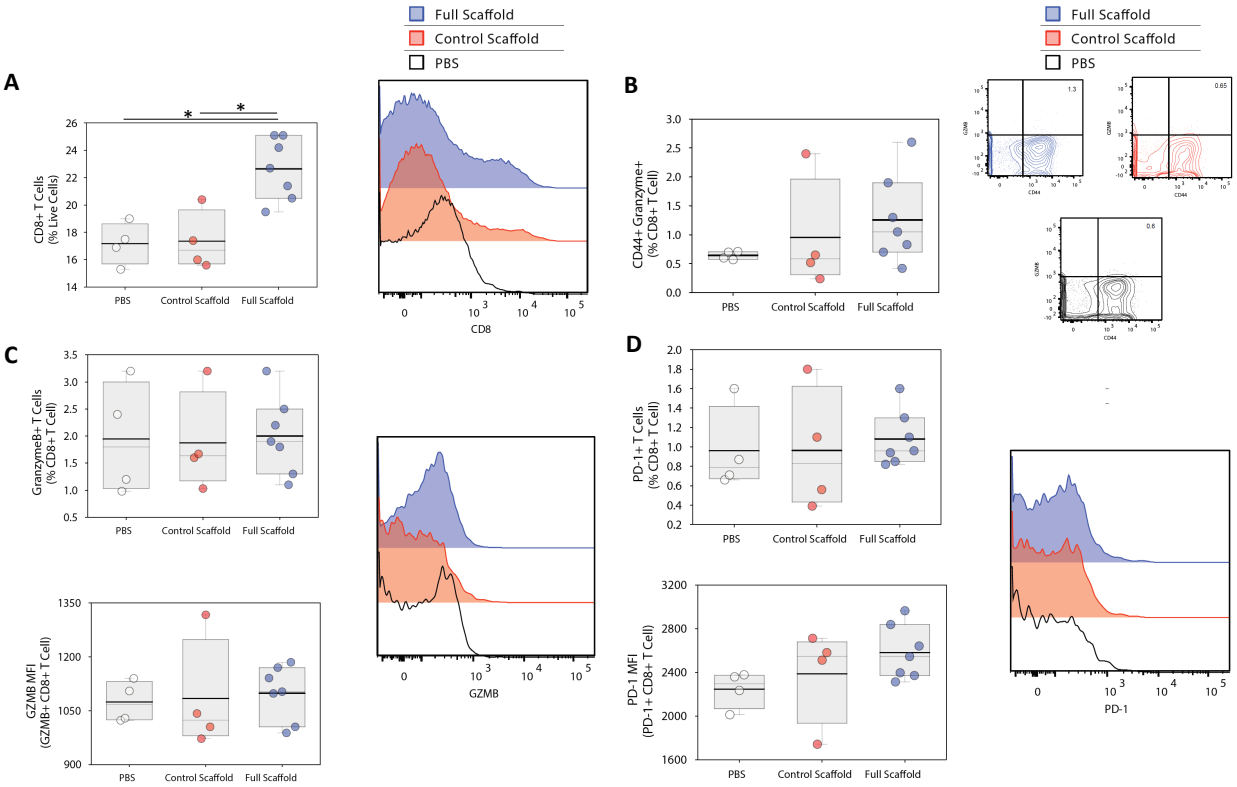

Supplementary Fig. 17 | No major effects on T cells in CD8+ T cells in Spleen. (A) Flow cytometry analysis of the percentage of CD8+ T cells in the spleen of tumor-bearing mice 22 days after subcutaneous injection of B16F10-ova cells for mice with different treatments. **(B)** Flow cytometry analysis of T cell activation is studied 22 days after inoculation of tumor cells. Percentage of GZMB+CD44+ T cells was similar in treated vs untreated conditions accompanied with their FACS representatives **(C)** Percentage of T cells with high intracellular expression of GZMB and mean fluorescence intensity (MFI) of T cells upregulating GZMB were plotted alongside with representative flow cytometry graphs. **(D)** Percentage of PD-1 expressing T cells and their MFIs gated on PD-1+ T cells were plotted. Representative flow cytometry graphs also presented. Each point represents one mouse.

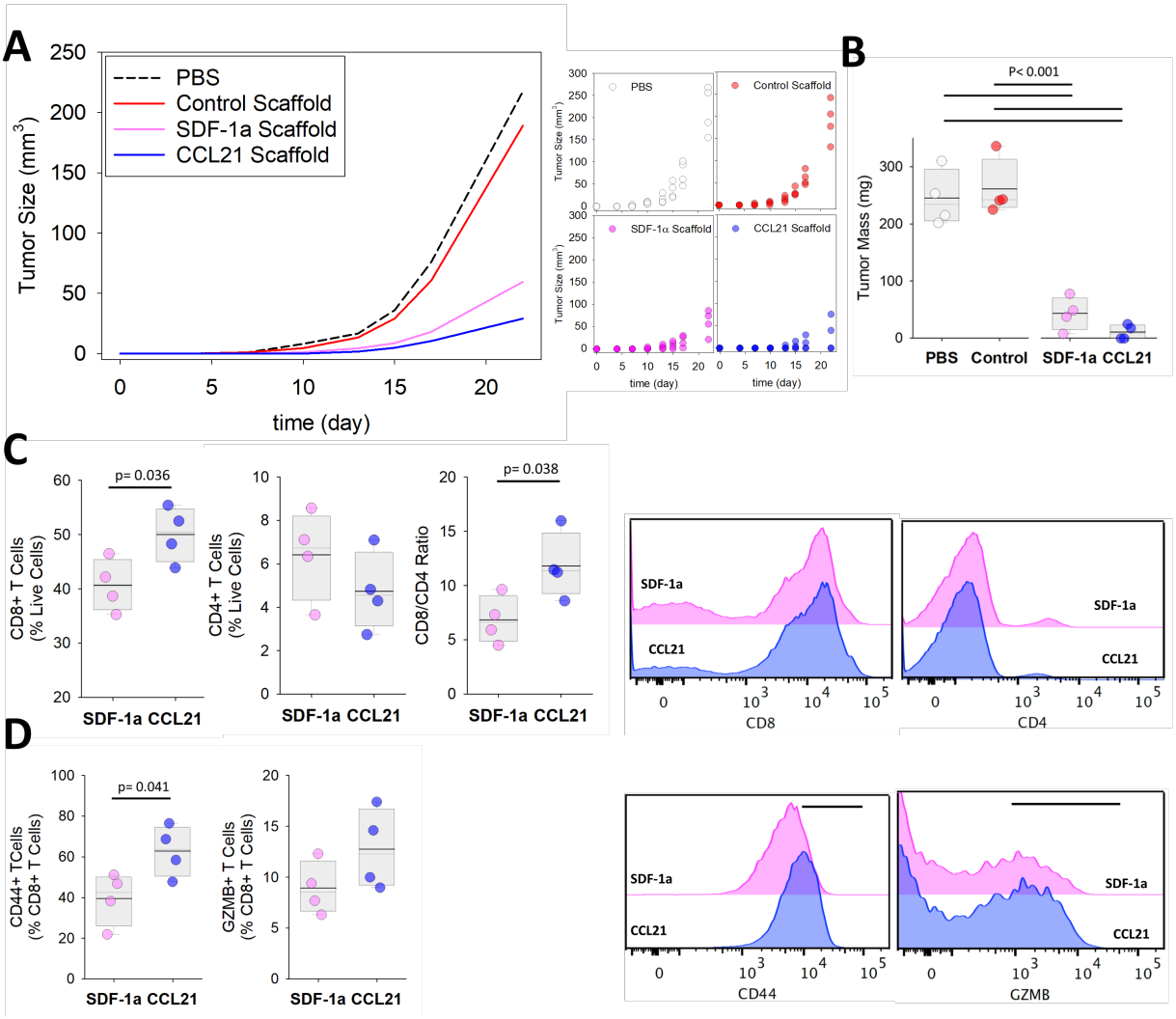

Supplementary Fig. 18 l Different chemokines in the scaffold can alter the recruitment of endogenous T cells and clearance of tumors. (A) Melanoma (B16-F10-Ova) tumor growth in wild-type mice with functionalized scaffolds, control scaffolds or PBS treatment (n= 4-7). The therapeutic effects of two chemokines (CCL21 and SDF-1a) were studied by assessing tumor growth over time. **(B)** Tumor masses were measured 22 days after tumor inoculation in wild-type mice treated with functionalized or control scaffolds or PBS treatment. **(C)** Flow cytometry analysis of CD4+ and CD8+ T cells recruited by the scaffolds 17 days after subcutaneous implantation of functionalized scaffolds releasing either CCL21 or SDF-1a chemokines (n=4). FACS quantification of CD8-to-CD4 ratio of recruited T cells extracted from immunoactive and control scaffolds. **(D)** The frequency of activated CD44+CD8+ and GZMB+CD8+ in scaffolds after treating mice with functionalized Scaffolds releasing either CCL21 or SDF-1a chemokines (n=4). Representative flow cytometry data were provided. Each point represents one mouse.

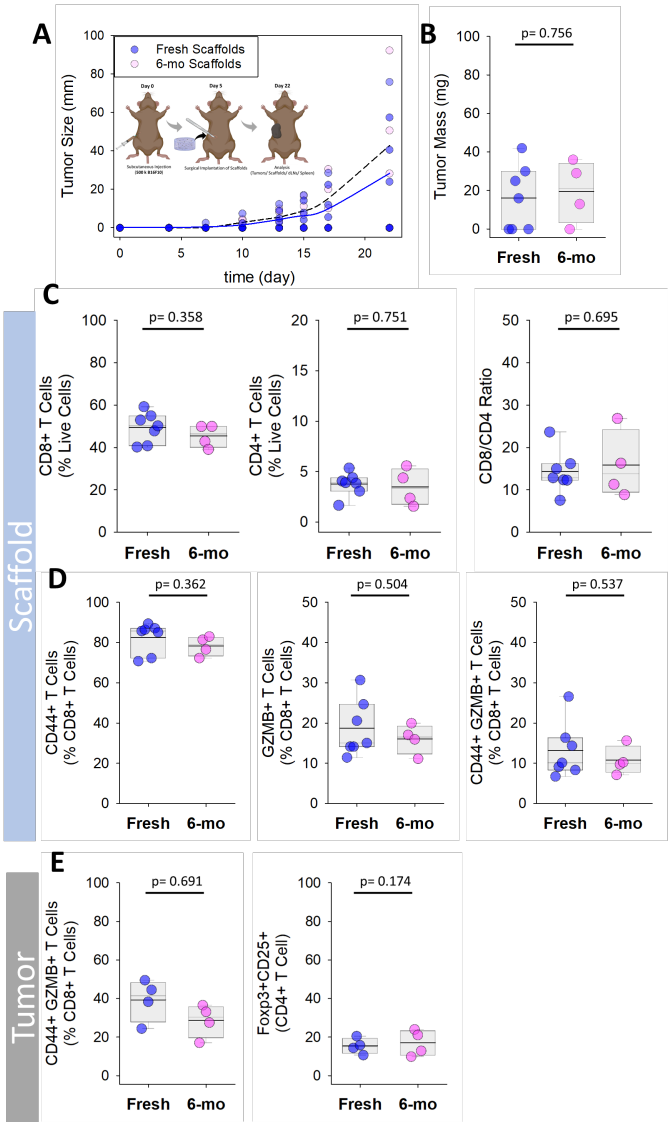

Supplementary Fig. 19 l Engineered scaffolds can preserve their therapeutic function several months after fabrication. (A) Melanoma (B16-F10-Ova) tumor growth. Inset: Timing of tumor inoculation and follow up surgical implantation of cells-free scaffolds. **(B)** Final tumor masses were measured 22 days after tumor inoculation in wild-type mice treated with fresh or 6-month old (immunoactive) scaffolds (n= 4-7). Each point represents a mouse. **(C)** Recruitment and activation of endogenous CD8+ and CD4+ T cells in freshly prepared and 6-Months old scaffolds. Flow cytometry analysis of percentage of CD8+, and CD4+, ratio of CD8+/CD4+ T cells **in the scaffolds**. (D) The frequency of activated CD8+ T cells in the scaffolds assessed by CD44, granzyme B, as well as co-expression of CD44 and granzyme in T cells after freshly prepared or 6-months old Immunoactive **Scaffolds**. **(E)** The frequency of activated CD44+GZMB+CD8+ and Foxp3+CD25+CD4+ Tregs in **tumors** after being treated with fresh or 6-month old Immunoactive Scaffolds. Each point represents one mouse.

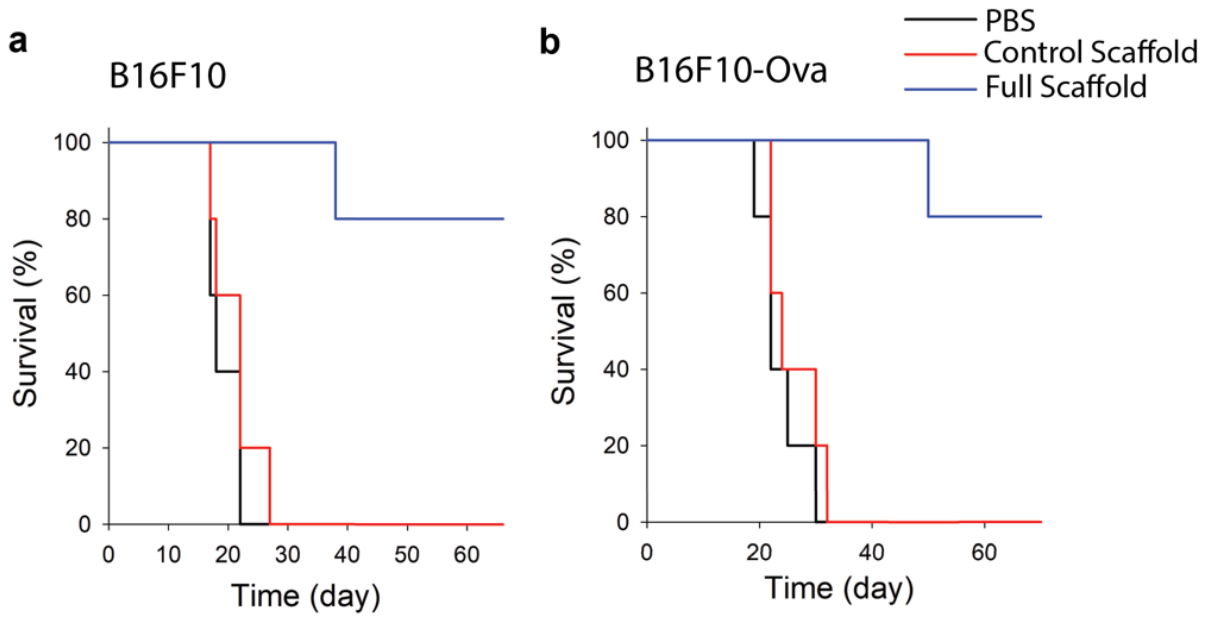

Supplementary Fig. 20 | Presence or absence of Ova will not affect progression and response of B16F10 melanoma *in vivo*. Survival of mice after subcutaneous injection of $5x10^5$ B16F10 or B16F10-Ova melanoma cells following treatment with either PBS, Blank Scaffold or immunoactive (Full) scaffolds.

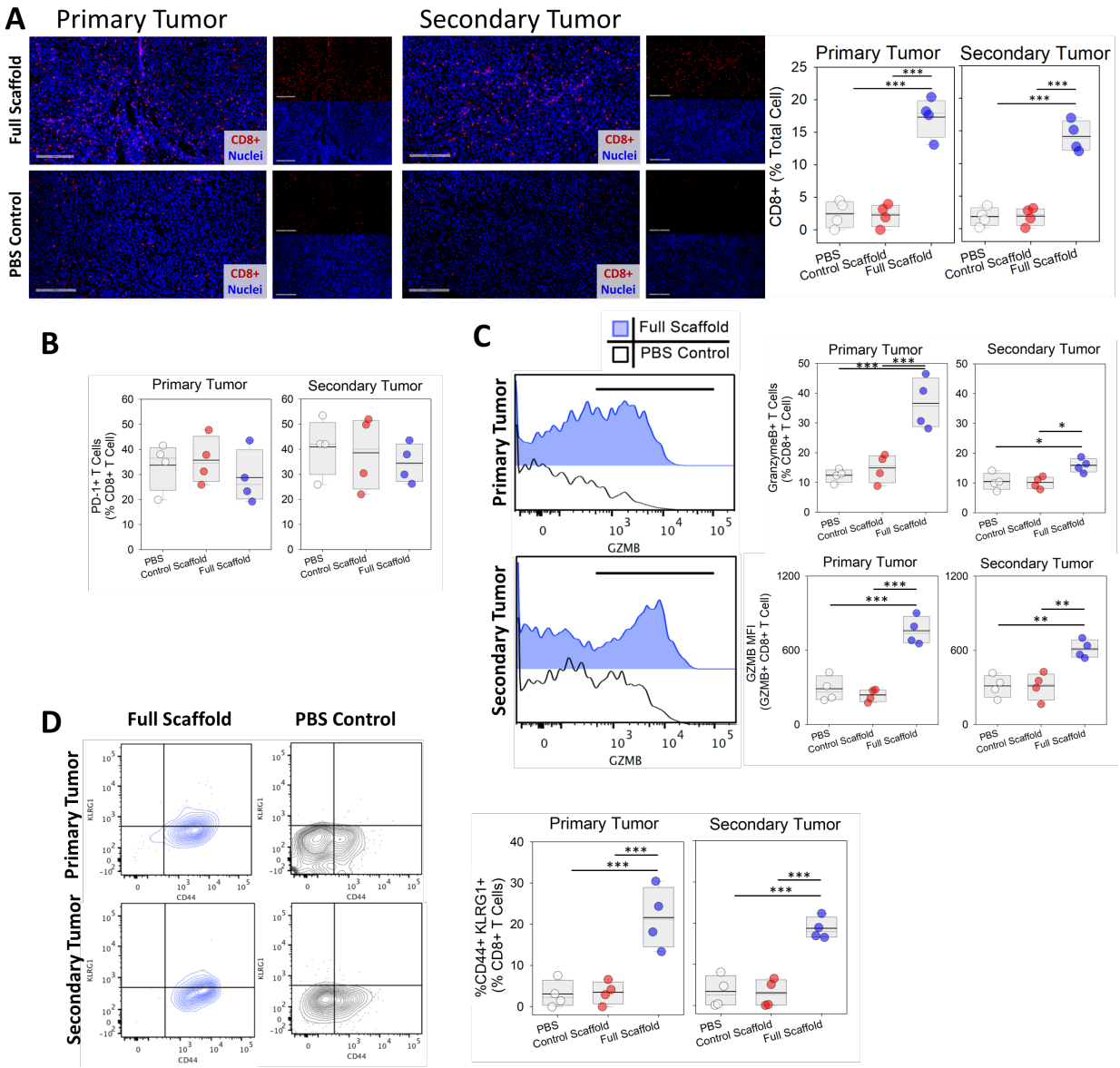

Supplementary Fig. 21 | Secondary tumor model, T cell activation <u>in the tumor</u>s. (A) Tumor-associated CD8+ T cells were stained in primary and secondary tumors 22 days after tumor inoculation. The frequency of CD8+ T cells **in tumors** were quantified and presented. **(B)** Flow cytometry study of PD-1+CD8+ T cells present in primary and secondary tumors after being treated with immunoactive or control scaffolds. **(C)** Flow cytometry study of GZMB+CD8+ T cell presence in primary and secondary tumors after being treated with immunoactive or control Scaffolds. The frequency and MFI of GZMB+CD8+ T cells in primary and secondary tumors. **(D)** Flow cytometry study of CD44+KLRG-1+CD8+ T cell presence in primary and secondary tumors after being treated with immunoactive or control Scaffolds. Representative FACS and frequency of CD44+KLRG-1+CD8+ T cells in primary and secondary tumors. Note: As 3 out of 7 mice treated with immunoactive scaffold formulation did not grow tumors, these representative sections were only found in the few mice with remaining tumors. (n=4). Each point represents one mouse.

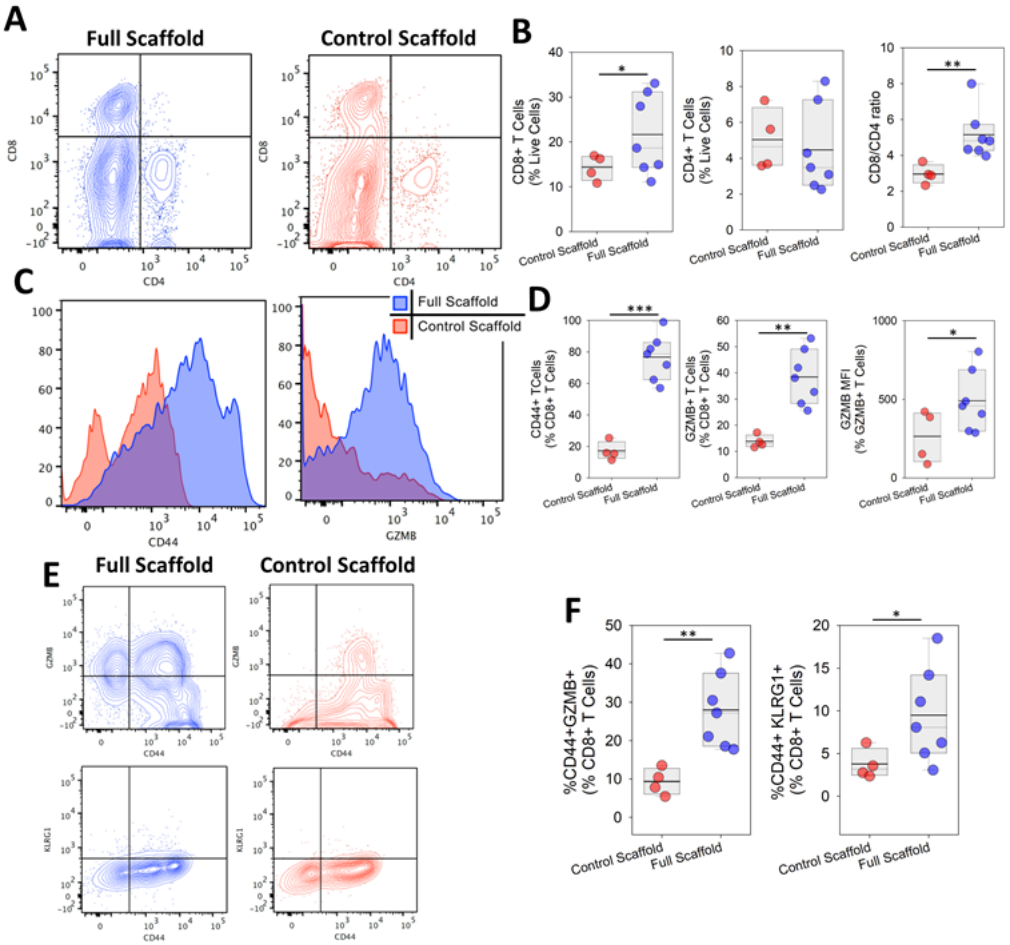

Supplementary Fig. 22. Secondary tumor model, T cell activation <u>in the scaffolds</u>. (A) Flow cytometry study of CD8+ T cell presence **in scaffolds** implanted adjacent to tumors. **(B)** The frequency of CD8+ and CD4+ T cells as well as the CD8-to-CD4 T-cell ratios in immunoactive (n=7) and control scaffolds (n=4). **(C-D)** Flow cytometry study of CD44+CD8+ and GZMB+CD8+ T cell presence in scaffolds 17 days after being implanted in tumor-bearing mice. (C) Representative FACS and (D) frequency of CD44+CD8+ and GZMB+CD8+T cells as well as MFI of GZMB+CD8+ T cells in immunoactive (n=7) and control (n=4) scaffolds. **(E-F).** Flow cytometry study of CD44+KLRG-1+CD8+ T cell presence in scaffolds 17 days after being implanted in tumor-bearing mice. (E) representative FACS and (B) the frequency of (F) CD44+KLRG-1+CD8+ T cells in Immunoactive (n=7) and Control (n=4) scaffolds.

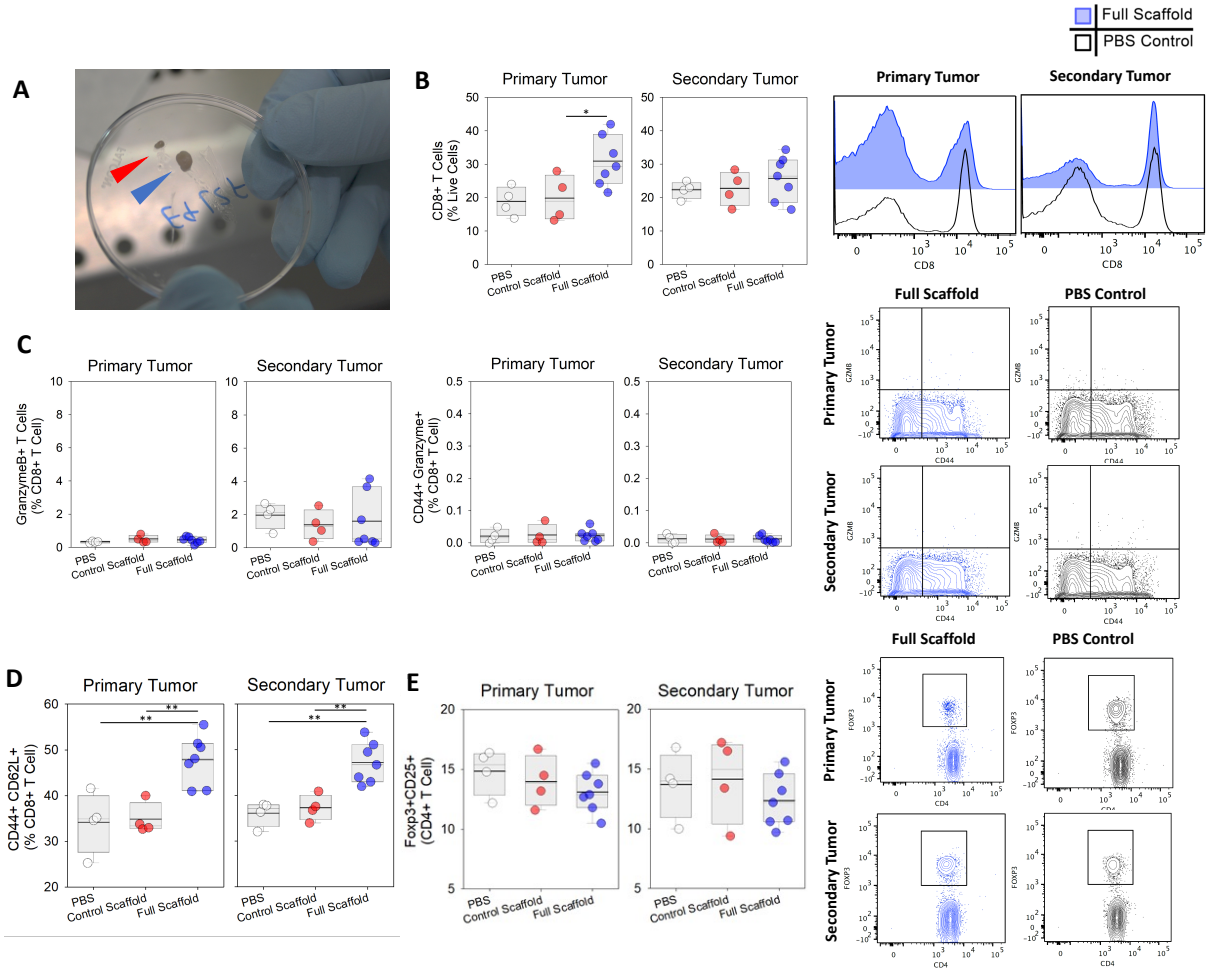

Supplementary Fig. 23 l Secondary tumor model, T cell activation <u>in the draining lymph nodes</u>, after being treated with immunoactive (n=7) or control (n=4) scaffolds. **(A)** Showing typical images of primary draining lymph nodes of animal treated with either with immunoactive (blue arrow) or control (red arrow) scaffolds. **(B)** Representative FACS graphs and the frequency of CD8+ T cells in draining lymph nodes of primary and secondary tumors. **(C)** Flow cytometry study of GZMB+CD8+ T cell presence in draining lymph nodes of primary and secondary tumors after being treated with immunoactive (n=7) or control (n=4) Scaffolds. The frequency of GZMB+CD8+ T cells in draining lymph nodes of primary and secondary tumors. Flow cytometry study of CD44+GZMB+CD8+ (effector) T cell presence in draining lymph nodes of primary and secondary tumors after being treated with immunoactive (n=7) or control (n=4) Scaffolds. **(D)** Flow cytometry study of the frequency of CD44+CD62L+CD8+ (central memory) T cell presence in draining lymph nodes of primary and secondary tumors after being treated with immunoactive (n=7) or control (n=4) scaffolds. **(E)** The quantified frequency of Foxp3+CD25+CD4+ Tregs found in tumor draining lymph nodes. Representative flow cytometry of Foxp3+CD25+CD4+ Tregs in primary and secondary tumor draining lymph nodes for mice treated with immunoactive scaffolds (Blue) and PBS (Black).

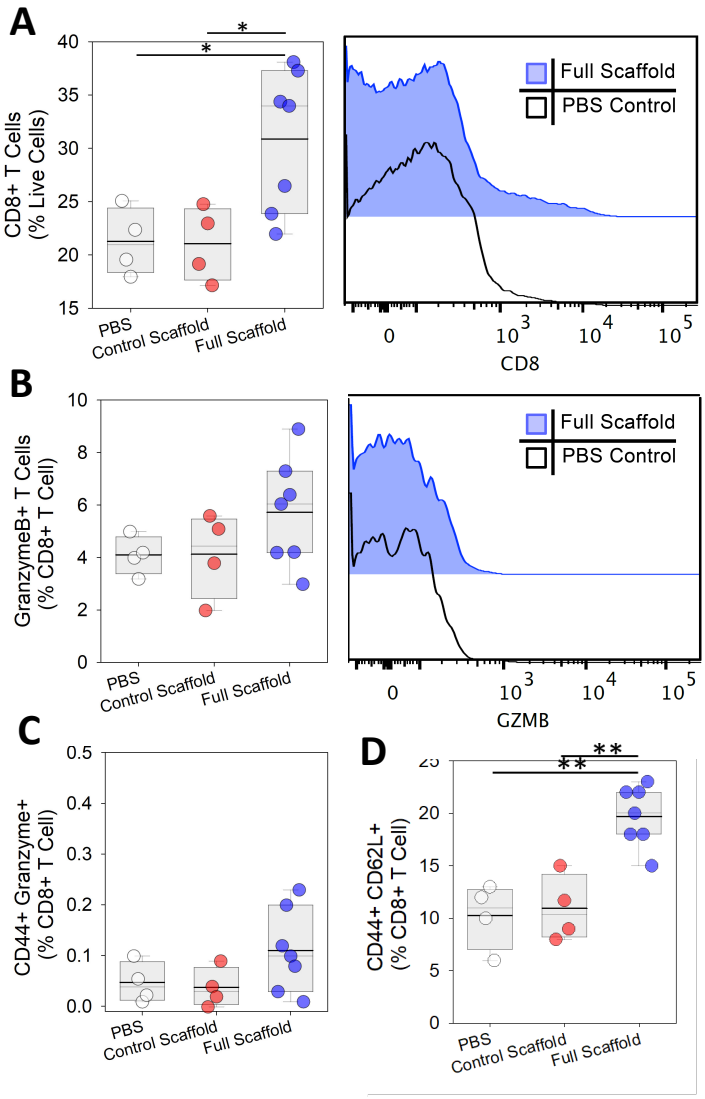

Supplementary Fig. 24 l Secondary tumor model, T cell activation <u>in the spleen</u>. Flow cytometry study of CD8+ T cell presence in the spleen of mice after being treated with immunoactive (n=7) or control (n=4) scaffolds. **(A)** The frequency of CD8+ T cells and representative FACS graphs. **(B)** Representative FACS graphs and frequency of GZMB+CD8+ T cells in the spleen. The frequency of **(C)** CD44+GZMB+CD8+ (effector) and **(D)** CD44+CD62L+CD8+ (central memory) T cells in the spleen.

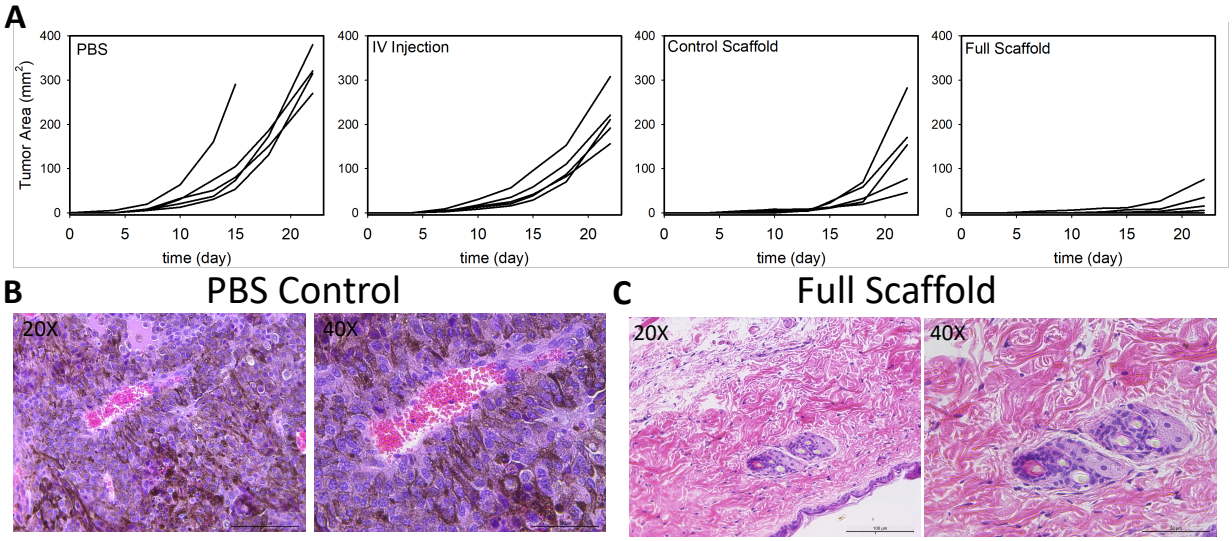

Supplementary Fig. 25 l Adoptive T cell model, tumor growth and histology. (A) Melanoma (B16-F10-Ova) tumor growth for groups with different treatments. Each line represents the tumor size of a single mouse over time. **(B-C)** Histologic analysis of the tumor tissues via H&E stain for animals used as **(B)** PBS control *vs.* **(C)** OT-I-loaded Immunoactive Scaffolds.

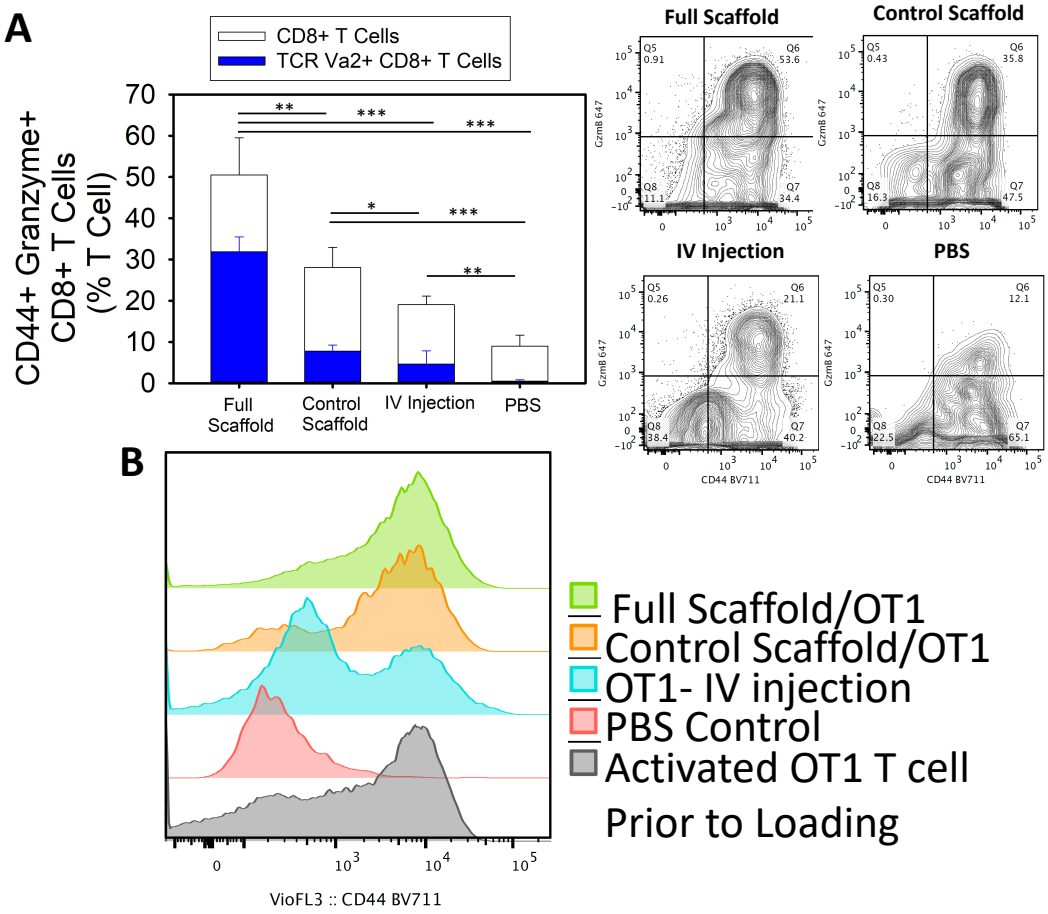

Supplementary Fig. 26 l Adoptive T cell model, presence of activated CD8+ T cells <u>in tumors</u>. (A) Presence of activated tumor-antigen specific (OT1) CD8+ T cells as well as CD8+ T cells in the tumors was studied 22 days after inoculation of tumor cells using flow cytometry. Percentage of T cells with high expression of CD44 activation marker and GZMB effector cytokine were plotted. Representative flow cytometry graphs also presented. (n= 5). **(B)** Flow cytometry used to identify the presence of activated (CD44 expressing) CD8+ T cells in tumors.

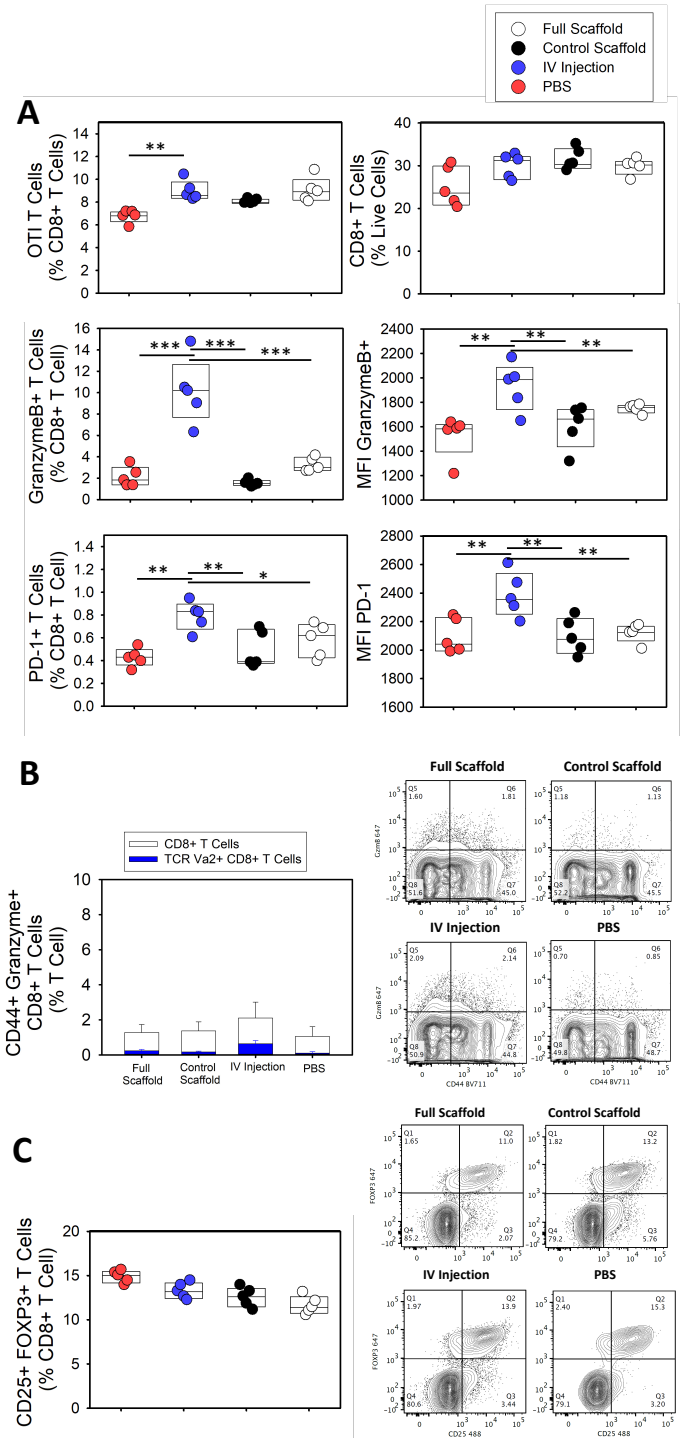

Supplementary Fig. 27 l Adoptive T cell model, presence of activated CD8+ T cells in <u>tumor draining lymph nodes</u>. (A) Presence of tumor-antigen specific CD8+ T cells (OTI) as well as activation of CD8+ T cells in the tumor draining lymph nodes was studied 22 days after inoculation of tumor cells using flow cytometry. Percentage of OTI and CD8+ T cells found in tumor draining lymph nodes. Frequency of CD8+ T cells with high expression of GZMB and PD-1 and mean fluorescence intensity (MFI) of T cells upregulating these two proteins were measured. (n= 5). **(B)** Presence of tumor-antigen specific CD8+ T cells as well as activation of CD8+ T cells in the tumor draining lymph nodes was studied 22 days after inoculation of tumor cells using flow cytometry. Percentage of T cells with high expression of CD44 activation marker and GZMB effector cytokine were plotted. Representative flow cytometry graphs also presented. (n= 5). **(C)** The frequency of Foxp3+CD25+CD4+ Tregs in tumor draining lymph nodes were studied. Representative flow cytometry graphs also presented (n= 5).

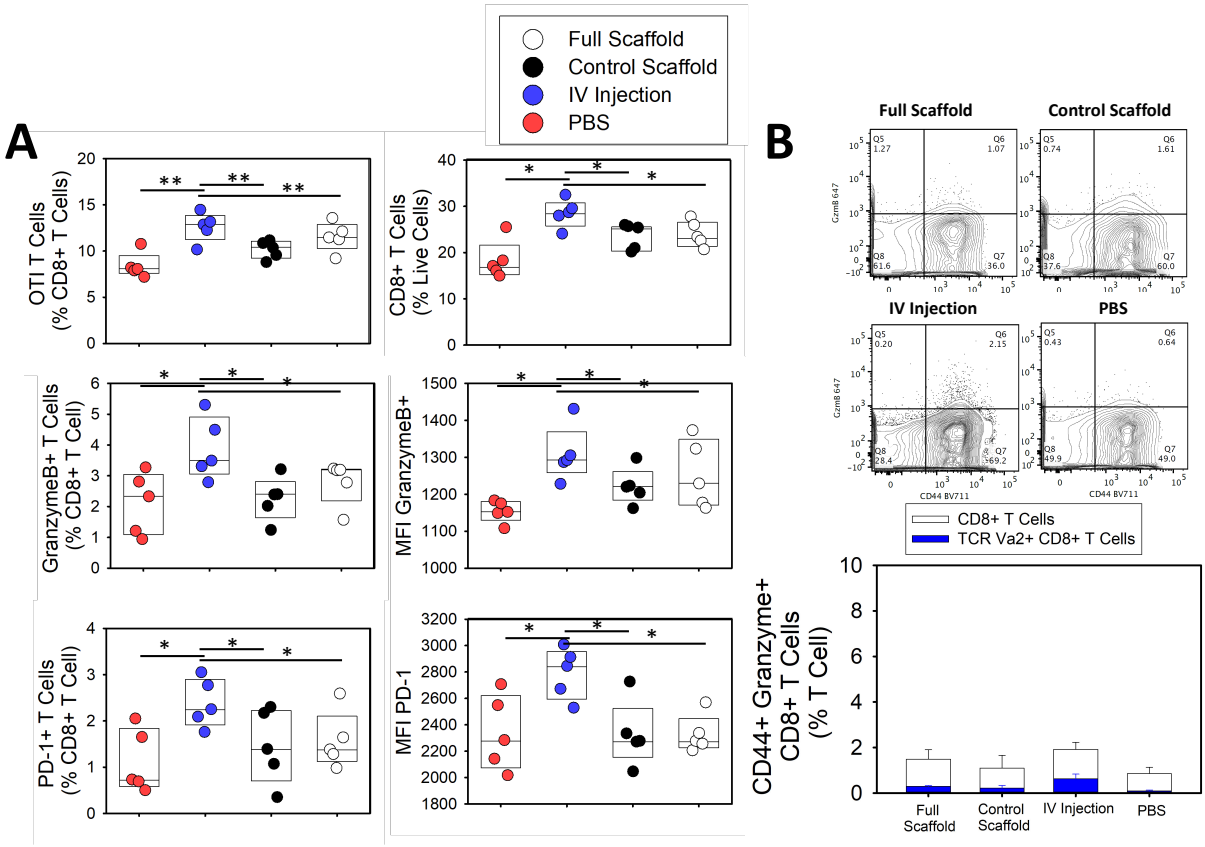

Supplementary Fig. 28 l Adoptive T cell model, presence of activated CD8+ T cells <u>in spleen</u>. (A) Presence of tumor-antigen specific CD8+ T cells (OTI) as well as activation of CD8+ T cells in the spleen of tumor bearing mice was studied 22 days after inoculation of tumor cells using flow cytometry. (A) Percentage of OTI and CD8+ T cells found in spleen. Frequency of CD8+ T cells with high expression of GZMB and PD-1 and mean fluorescence intensity (MFI) of T cells upregulating these two proteins were measured. **(B)** Presence of tumor-antigen specific CD8+ T cells as well as activation of CD8+ T cells in the spleen of tumor bearing mice was studied 22 days after inoculation of tumor cells using flow cytometry. Percentage of T cells with high expression of CD44 activation marker and GZMB effector cytokine were plotted. Representative flow cytometry graphs also presented. (n= 5).

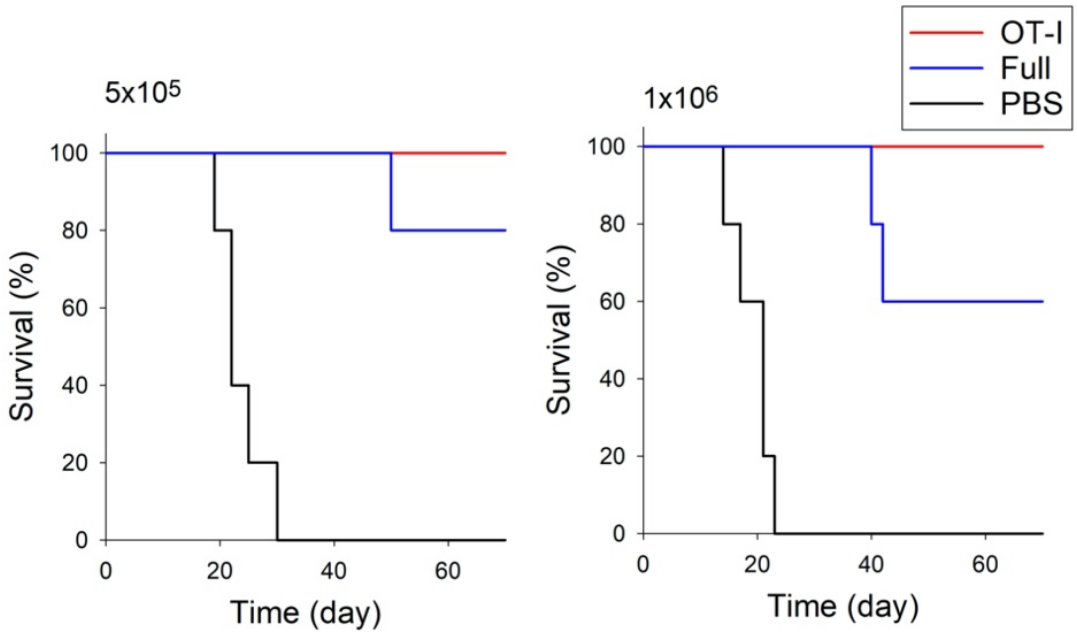

Supplementary Fig. 29 | Therapeutic advantage of T cell delivery in a stablished melanoma tumor. Survival of mice after subcutaneous injection of either $5x10^5$ or $1x10^6$ B16F10-Ova melanoma cells followed by treatment with immunoactive (Full) scaffolds in the presence or absence of loaded OT1 T cells, or PBS (control) injection.

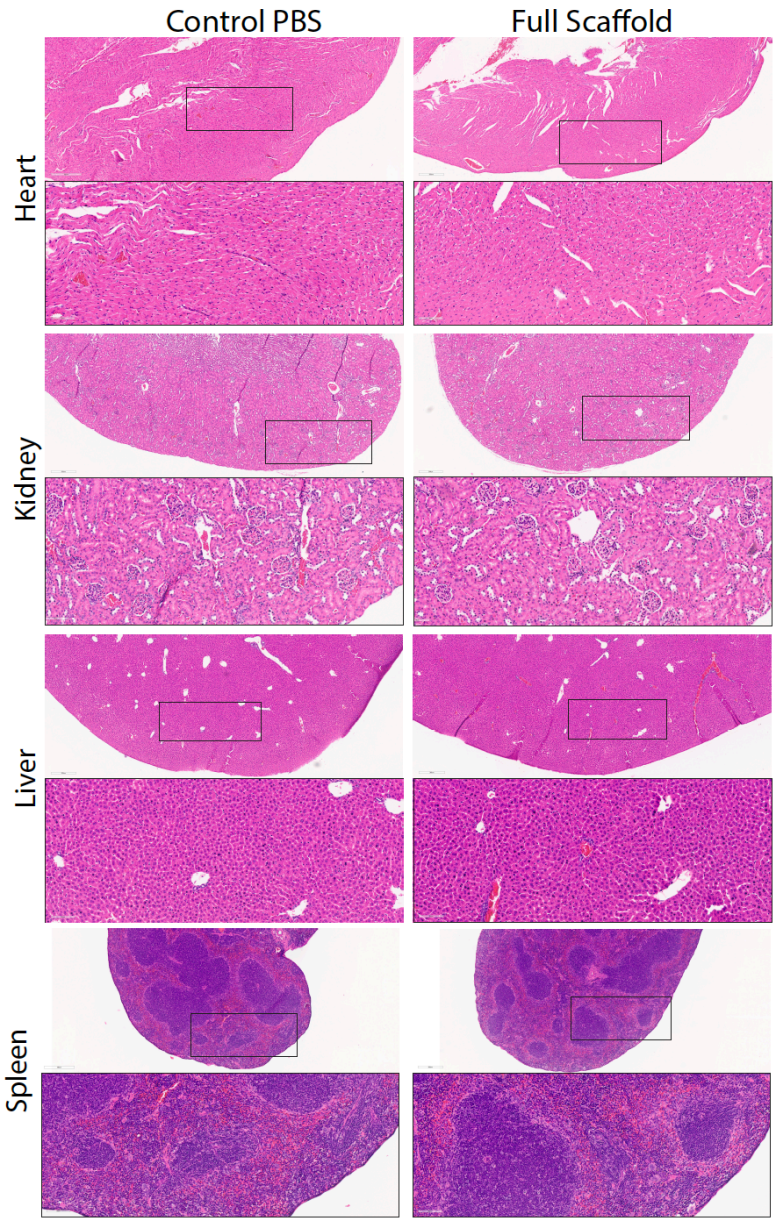

Supplementary Fig. 30 l Biosafety evaluation of Full scaffold. Histology analysis of the major organs of mice 7 days after surgical implantation of the Full scaffolds. Images are presented in two magnifications.

Supplementary Table 2 | Biosafety evaluation of Full scaffold. Blood chemistry and hematology for naïve mice treated with either PBS injections (Control) or with implanted Full scaffolds 7 days post-implantation.

CLINICAL CHEMISTRY	Control	Full
ALP (U/L)	110±23	96±18
AST (U/L)	189±46	214±64
ALT (U/L)	39±17	47±20
Creatine kinase (U/L)	1992±723	2309±672
Albumin (g/dL)	2.7±0.4	2.8±0.3
Total Bilirubin (mg/dL)	0.2±0.03	0.2±0.01
Total Protein (g/dL)	4.4±0.3	4.5±0.4
Globulin (g/dL)	1.6±0.2	1.7±0.3
BUN (mg/dL)	21±4.3	23±2.1
Creatinine (mg/dL)	0.2±0.02	0.17±0.03
Cholesterol (mg/dL)	72±5	77±6.9
Glucose (mg/dL)	152±15	137±20
Calcium (mg/dL)	8.3±0.78	7.8±0.5
Phosphorus (mg/dL)	13.5±2	14.2±1.3
Bicarbonate TCO2 (mmol/L)	8.7±1.1	9.6±1.3
Chloride (mmol/L)	116±5.6	114±7
Potassium (mmol/L)	4.7±0.9	5.3±0.8
ALB/GLOB ratio	1.85±0.26	1.65±0.2
Sodium (mmol/L)	149±5.1	154±7.2
NA/K Ratio	31±4.9	28±6.2
HEMATOLOGY		
WBC (K/uL)	1±0.23	1.3±0.33
RBC (M/uL)	8.78±0.48	8.45±0.56
HGB (g/dL)	14.1±0.91	13.7±1.8
HCT (%)	41.1±3.9	38.4±3.4
MCV (fL)	47±4.7	48±3.8
MCH (pg)	16.1±0.6	17.3±0.9
MCHC (g/dL)	34.8±4.8	37.8±5
Platelet Count (K/uL)	1018±245	1209±319
Neutrophil (/uL)	108±48	128±31
Lymphocyte (/uL	895±254	1032±301
Monocyte (/uL)	56±21	78±23
Eosinophil (/uL)	0	0
Basophil (/uL)	0	0

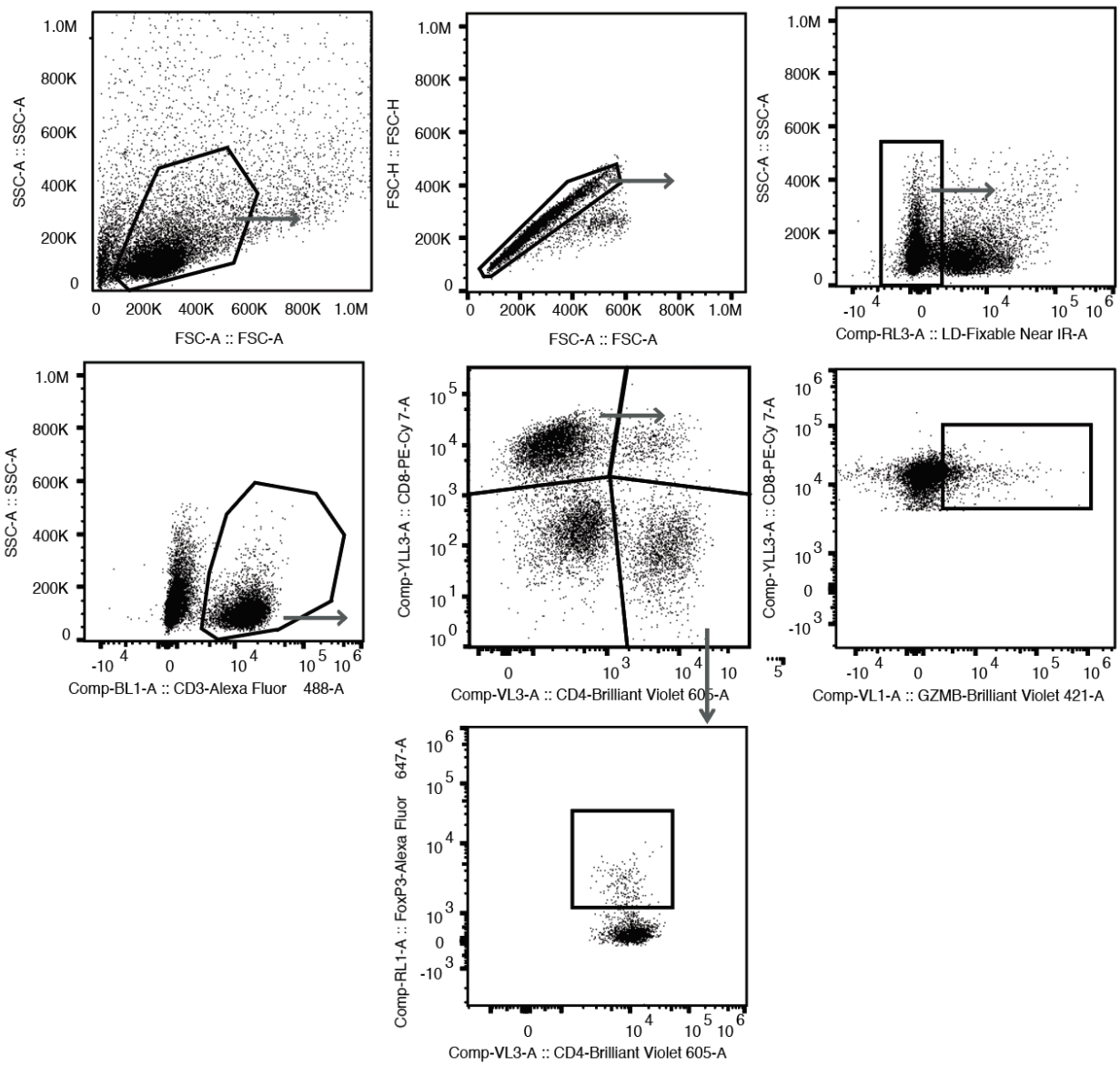

Supplementary Fig. 31 | Representative Gating Strategy for identifying T cell populations.